EPR spectra of separated pairs of substitutional nitrogen atoms in diamond with a high concentration of nitrogen

V. A. Nadolinny
Institute of Inorganic Chemistry, Novosibirsk 630090, Russia

A. P. Yelisseyev
Institute of Mineralogy and Petrography, Novosibirsk 630090, Russia

J. M. Baker,* D. J. Twitchen, and M. E. Newton
Department of Physics, University of Oxford, Clarendon Laboratory, Parks Road, Oxford OX1 3PU, United Kingdom

A. Hofstaetter
Das I Physikalishes Institut, Justas-Liebig Universitat, Giessen, Germany

B. Feigelson
Research Centre Basis, Facultetskiy per. 12, Moscow 125080, Russia
(Received 9 February 1999)

Electron paramagnetic resonance (EPR) measurements are reported in synthetic diamonds grown in an Fe-Ni-C solvent/catalyst system at 1750 K, under stabilizing pressure, by the temperature gradient method. Such diamonds are known to have high concentrations of nitrogen. EPR spectra have been found in three well-separated regions. The first of these spectra consists of a family of lines around the EPR spectrum of the $P1$ center (isolated N_s). The second spectrum consists of a family of weak lines at about one-half of the $P1$ magnetic field. The third consists of a family of weak lines at about twice the $P1$ magnetic field. The first spectrum is attributed to three defect centers, named NOC1, NOC2, and NOC3 (NOC stands for the Novosibirsk-Oxford collaboration) ; each one of the centers corresponds to a pair of N_s atoms with different separations. The second spectrum, named NOC4, is also attributed to separated pairs of N_s atoms, but is a superposition of spectra from all pairs with separation greater than about 0.7 nm. The third spectrum is attributed to isolated $P1$ centers which were resonated by a two microwave photon transition.
[S0163-1829(99)09031-1]

I. INTRODUCTION

There is interest in defects and impurities in diamond because of the influence they have upon material properties and the information their presence provides on growth conditions. Substitutional nitrogen atoms, N_s, are known to be a constituent of many defect centers in diamond, with complexity varying from the $P1$ center (isolated N_s),[1] to centers involving up to at least five N_s atoms.[2–4] Synthetic diamonds usually contain nitrogen in the form of isolated, paramagnetic N_s; but for the majority of natural diamonds the most common nitrogen forms are A centers (nearest-neighbor pairs N_s-N_s) or B centers (four N_s arranged around a vacancy) both of which are diamagnetic,[5,6] and the paramagnetic $P2$ center (three N_s around a vacancy).[3] Several other complexes of N_s have been identified involving vacancies, and are formed following radiation damage and annealing.[2,6]

The aggregation of isolated N_s atoms to form A centers, and of A centers to form B centers, has been extensively studied at temperatures between 1800 and 2500 K.[7–9] Chrenko *et al.*[7] found that the aggregation of isolated N_s atoms to form A centers followed second-order kinetics. Subsequent studies have shown that the presence of vacancies[10] and impurities, such as nickel and cobalt,[11,12] can dramatically increase the rate of aggregation. Vacancy-enhanced aggregation at 1800 K was studied by Collins,[10] who proposed that the aggregation process can involve the multiple release and retrapping of vacancies. Fisher and Lawson[12] have shown that the preferential incorporation of nickel and cobalt in {111} growth sectors enhances the aggregation of isolated N_s to form A centers in these sectors, with the degree of enhancement increasing with increasing nickel/cobalt content. A marked deviation from simple second-order kinetics was observed in these sectors. Synthetic diamonds grown in an Fe-Ni-C solvent/catalyst system contain substitutional nickel (Ni_s) as well as N_s. Annealing under stabilizing pressure results in aggregation of N_s with Ni_s to form a range of complexes $NE1$–7.[13–16]

This study reports new measurements on synthetic diamonds grown in an Fe-Ni-C solvent/catalyst system at 1750 K, under stabilizing pressure, by the temperature gradient method. EPR spectra have been found in three well-separated regions of magnetic field. They are much weaker than the EPR spectrum of the $P1$ center (known to be an isolated N_s atom with $g=2.0024$), but they are shown to be related to N_s atoms. All but one of the new spectra are from pairs of N_s atoms and the other arises from a transition in N_s driven by two photons. The models for these centers are discussed in Secs. III–V.

II. EXPERIMENT

A. Synthetic diamond samples

The synthetic diamonds used in this work were grown in an iron-nickel solvent/catalyst system at temperatures and pressures in the region of 1750 K and 5.5 GPa, respectively, using a multianvil split-sphere ultrahigh pressure apparatus.[17,18] The diamond crystals showed an octahedral growth habit, and were light yellow in color. Infrared-absorption measurements, which sample about 50% of the diamond surface, indicate that the samples contain both $P1$ and A centers; the samples were therefore characterized as mixed Ib/IaA. The concentration of $P1$ and A centers was somewhat inhomogeneous, both within one sample and between samples. Decomposition of the measured infrared-absorption spectra into its component spectra indicated that between samples the concentration of $P1$ centers ranged between 80 and 200 parts per million (ppm) carbon atoms (in accord with EPR intensity measurements), and the concentration of A centers ranged between 20 and 120 ppm. EPR measurements indicated that the typical concentration of Ni_s ($W8$) (Refs. 19–21) was 2–10 ppm, and of defects $NE1$–NE[13] was 0.01–1 ppm.

The line width of the EPR of $P1$ ($\sim$0.3 mT) indicated that the local concentration of N_s in the region contributing to the EPR spectrum was about 300 ppm.[22,23] This indicates that the local density of N_s in some regions was larger than indicated by the EPR intensity and IR absorption. The high concentration of A centers showed that the distribution for very close neighbors was clearly not statistical.

B. Equipment

EPR spectra were recorded at temperatures ranging from 4.2 to 300 K with Varian and Bruker spectrometers operating at an X band (nominally $\sim$9.6 GHz). Low temperatures were achieved using an Oxford Instruments ESR900 cryostat. Measurements were made with the applied **B** field rotated in a {110} plane, where all principal high-symmetry directions can be accessed. The precise orientation of the crystal in the applied magnetic field **B** was determined using the well-documented $P1$ spectrum.[1,24]

C. Spectrum

The measured spectrum has three distinct parts: (a) a family of weak lines centered at $g=2.0024(1)$ in the wings of $P1$ which has a strong three line spectrum with the same g value (see Fig. 1). We identify three centers (see Sec. IV) which we label NOC1, NOC2, and NOC3, where NOC stands for the Novosibirsk-Oxford collaboration, in the spirit of the convention for labeling EPR centers in diamond;[2] (b) a spectrum at about half of the magnetic field needed for spectrum (a), which we label NOC4 (see Fig. 2); and (c) a replica of the spectrum of $P1$ at approximately twice the magnetic field needed for spectrum (a) (see Fig. 3), which we label the high-field spectrum since we believe that the P1 center is responsible for it, rather than some new center. More details of these spectra and their interpretation are presented in Secs. III–V.

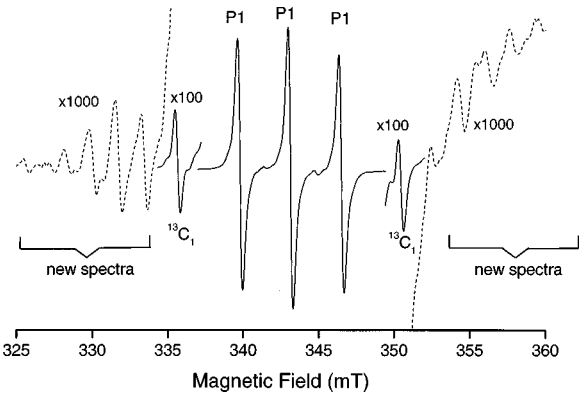

FIG. 1. The EPR spectrum of the $P1$ center and the weak new spectra in its wings for **B** along the ⟨001⟩ crystallographic axis. The microwave frequency was approximately 9.6 GHz, and the measurements were made at room temperature. The outermost ^{13}C hyperfine lines from the unique carbon atom in the $P1$ center are labeled $^{13}C_1$, and shown at 100× magnification relative to the three central lines. The new spectra are shown at 1000× magnification relative to the three central lines.

D. EPR spectrum of $P1$

Since we believe that all of the spectra we obtain are related to the $P1$ center, which is the paramagnetic defect with by far the largest concentration in the samples, we briefly summarize its properties. The spin Hamiltonian describing the $P1$ EPR spectrum is well known:[1]

$$\mathcal{H}=g\mu_B\mathbf{B}\cdot\mathbf{S}+\mathbf{S}\cdot\mathbf{A}\cdot\mathbf{I}, \tag{1}$$

where $S=1/2$, the second term describes the hyperfine interaction with the ^{14}N nucleus with $I=1$, and **A** is axially symmetric about a ⟨111⟩ axis. We have assumed the electronic g value to be isotropic (a reanalysis of published data[25] indicates that anisotropy is less than 0.000 03), and we have ignored the nuclear Zeeman interaction $g_N\mu_N\mathbf{B}\cdot\mathbf{I}$ and the quadrupole interaction $\mathbf{I}\cdot\mathbf{P}\cdot\mathbf{I}$, which to first order do not influence the EPR spectrum. The separation of hyperfine lines

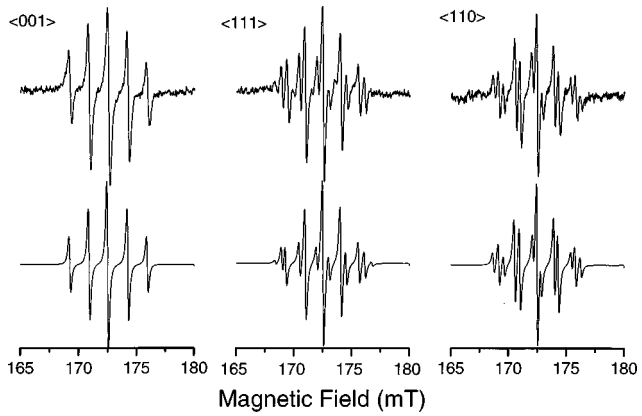

FIG. 2. The EPR spectra for NOC4 near half of the magnetic field shown in Fig. 1 for **B** along ⟨100⟩, ⟨111⟩, and ⟨011⟩ crystallographic directions. The experimental data (upper spectra) can be compared with simulated spectra (lower spectra). The microwave frequency was approximately 9.7 GHz, and the measurements were made at approximately 5 K.

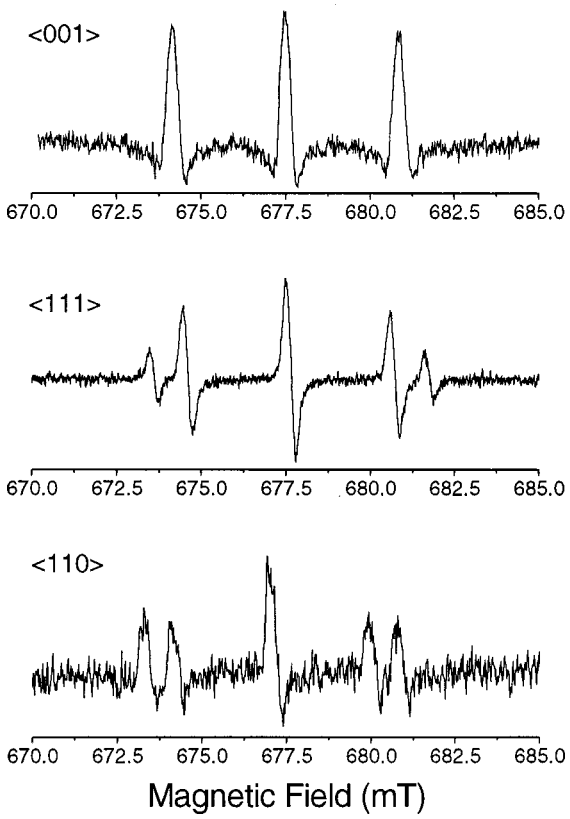

FIG. 3. The EPR spectra near twice the magnetic field shown in Fig. 1. Experimental data are shown for **B** along the ⟨100⟩, ⟨111⟩, and ⟨011⟩ crystallographic directions. The microwave frequency was approximately 9.5 GHz, and the measurements were made at 5K.

for various directions of the applied magnetic field **B** are given in Table I, and the spin Hamiltonian parameters are given in Table II. There are also weak lines due to hyperfine interaction with neighboring ^{13}C nuclei ($I=\frac{1}{2}$) of 1.1% natural abundance (shown and labeled in Fig. 1).

The observed EPR spectrum comprises a superposition of spectra for four symmetry-related sites. The separation of the hyperfine lines for these differently oriented sites is shown in Table I. The separation listed first under ⟨111⟩ and ⟨110⟩ corresponds to parallel and perpendicular to the axis, respectively. For the separations at listed angles θ in the {110} plane, those which are nondegenerate correspond to axes which lie in the plane, and the doubly degenerate ones have axes which lie out of the plane.

The site is axially symmetric because the unpaired electron goes preferentially into one of the N-C antibonding orbitals, which causes this orbital to be elongated by about 30%.[26–28] The hyperfine interaction with its constituent ^{14}N and ^{13}C nuclei shows that 67% of the unpaired electron density in centered on C and 25% on N.[1]

E. EPR spectra of pairs of paramagnetic centers

Interactions between paramagnetic centers in a solid give rise to shifts in the line positions which, when summed over the interacting centers, contribute to the linewidth.[30,31] For example, the relationship between the EPR linewidth in diamond and the concentration c of $P1$ centers has been studied.[22] However, there are circumstances in which the interactions between specific pair sites produce shifts which are larger than the linewidth due to interaction with all of the other sites, in which case the EPR lines from these pairs have been resolved as weak satellites.[31–34] The satellites are weak

TABLE I. The separation of hyperfine lines, in mT, measured in the centers described in this paper, and those calculated from the known spin Hamiltonian parameters for the $P1$ center for comparison, for various directions (Dir.) of the applied magnetic field **B**. The experimental uncertainty is about 0.02 mT. For $P1$, the high-field spectrum, and NOC4, all symmetry-related sites are included; but for NOC1, NOC2, and NOC3 only one site is described. For the centers involving pairs of atoms (NOC1–NOC4) there are two columns representing the hyperfine separations for each component nucleus. Square brackets indicates the number [no.] of sites with coincident lines. * indicates the angle between the direction of **B** and ⟨001⟩ in the {110} plane.

Dir.	$P1$ [no.]	High-field spectrum	NOC4	NOC1	NOC2	NOC3
⟨001⟩	3.337 [4]	3.34	1.68 1.68	1.68 1.68	1.68 1.68	1.68 1.68
⟨111⟩	4.070 [1]	4.08	2.04 2.04			
	3.054 [3]	3.14	1.57 1.57			1.58 1.58
			2.04 1.57		2.00 1.58	
⟨110⟩	2.903 [2]	2.92	1.46 1.46			1.44 1.44
	3.722 [2]	3.72	1.86 1.86			
			1.86 1.46			
20°*	3.730 [1]			1.80 1.60		
	3.289 [1]					
	3.180 [2]					
35°*	3.954 [1]				1.90 1.44	
	3.200 [1]					
	2.902 [2]					
78.5°*	3.927 [1]					
	3.498 [1]					
	2.920 [2]					1.48 1.48

TABLE II. Spin Hamiltonian parameters for the centers discussed in the paper. A/h and D/h are in MHz. Θ is the angle between the principal direction of D and $\langle 001\rangle$ in the $\{110\}$ plane. The axes of $\mathbf{A}_1$ and $\mathbf{A}_2$ are specified for one particular set of sites with principal axes in the (110) plane and along $[110]$. The two or more sets of parameters for each center are discussed in the text; *the lowest line for each center gives the correct interpretation.*

Center	Model	S	g value	$A\parallel/h$	$A\perp/h$	Axes of $\mathbf{A}_1$	Axes of $\mathbf{A}_2$	D/h	Θ
$P1$		$\frac{1}{2}$	2.0024(1)	114.034	81.325				
High-field	simple spin $\frac{1}{2}$	$\frac{1}{2}$	1.0025(1)	57	41				
spectrum	two photon	$\frac{1}{2}$	2.0038(2)	114	82				
NOC4	simple spin $\frac{1}{2}$	$\frac{1}{2}$	4.0085(1)	114	82				
	$\Delta M=2$	1	2.0043(1)	57	41			0	
	coupled pair	$\frac{1}{2}+\frac{1}{2}$	2.0043(1)	114	82				
NOC1	simple spin 1	1	2.0024(1)	57	41	$[111]$	$[\bar{1}\bar{1}\bar{1}]$	31.3(1)	0.0(5)
	coupled pair	$\frac{1}{2}+\frac{1}{2}$	2.0024(1)	114	82				
NOC2	simple spin 1	1	2.0024(1)	57	41	$[111]$	$[\bar{1}\bar{1}1]$	40.8(1)	35.0(5)
	coupled pair	$\frac{1}{2}+\frac{1}{2}$	2.0024(1)	114	82				
NOC3	simple spin 1	1	2.0024(1)	57	41	$[\bar{1}1\bar{1}]$	$[\bar{1}1\bar{1}]$	31.7(1)	78.5(5)
	coupled pair	$\frac{1}{2}+\frac{1}{2}$	2.0024(1)	114	82	or $[\bar{1}\bar{1}\bar{1}]$	$[1\bar{1}1]$		

since, for a concentration c per atomic site of a paramagnetic center, there is a probability c that any neighboring atomic site is occupied by another paramagnetic center; so the probability of occupation of that pair site is $\frac{1}{2}c^2$. Hence the relative intensity of the EPR line of the pair is about a factor c lower than that of an isolated center.

III. HALF-FIELD SPECTRUM: NOC4

A. Spectrum

At $\sim$9.7 GHz, this spectrum consists of a group of lines centered at about 172 mT, whose central field position was isotropic. The structure of the group had a complex angular variation, but is simpler in the high-symmetry directions (see Fig. 2). The spectrum is actually a superposition of several spectra, each of which is a convolution of two, equally spaced three line hyperfine structures of equal intensity. The separation of these three line groups is listed in Table I. The angular variation of the spectrum can be adequately described by a spin Hamiltonian with $S=1/2$ ($g\sim 4$) and $I_1=I_2=1$,

$$\mathcal{H}=g\mu_B\mathbf{B}\cdot\mathbf{S}+\mathbf{S}\cdot(\mathbf{A_1}\cdot\mathbf{I_1}+\mathbf{A_2}\cdot\mathbf{I_2}), \tag{2}$$

where $\mathbf{A}_1$ and $\mathbf{A}_2$ are axially symmetric with the same principal values $A_\perp$ and $A_\parallel$, whose principal directions are along $\langle 111\rangle$ directions. The spin Hamiltonian parameters which correspond to this description are given in Table II under NOC4. The spectrum is a superposition of *sites* with all possible orientations of $A_{1\parallel}$ and $A_{2\parallel}$ along $\langle 111\rangle$ directions with random probability. The clearest signature of two similar nuclei is when the external magnetic field ($\mathbf{B}$) is along $\langle 100\rangle$, when all sites are equivalent, and the spectrum comprises five equally spaced lines with relative intensity 1:2:3:2:1, shown in Fig. 2. For a general direction, the position of the hyperfine line corresponding to nuclear spin quantum numbers m_1 and m_2 is shifted from the center of the spectrum by $(A_1m_1+A_2m_2)/g\mu_B$, where $A_i=(A_\parallel^2\cos^2\phi_i+A_\perp^2\sin^2\phi_i)^{1/2}$, and ϕ_i is the angle between $\mathbf{B}$ and the principal direction of $\mathbf{A}_i$. For the simple case when $\phi_1=\phi_2$ and $A_1=A_2=A$, the hyperfine shift equal to $A(m_1+m_2)/g\mu_B$ leads to the simple structure shown in Fig. 2 for $\mathbf{B}$ along $\langle 100\rangle$. The relative intensities depend upon the number of permutations for making a particular value of (m_1+m_2) from equally probable values of $m_i=+1,0,-1$. For $\mathbf{B}$ along $\langle 100\rangle$, all sites have the same ϕ_i. For $\mathbf{B}$ along $\langle 111\rangle$, one site (type X) has $\phi_i=0$ and the other three sites (type Y) all have $\phi_i=\cos^{-1}(1/3)$. The spectrum is more complicated because $\frac{1}{16}$ of the pairs have both types X, $\frac{9}{16}$ of the pairs have both types Y, and $\frac{6}{16}$ have mixed types with A_1 not equal to A_2. The situation for $\mathbf{B}$ along $\langle 110\rangle$ can be deduced similarly. However, the spectra all correspond to patterns expected for a random distribution over the possible orientations. Figure 2 shows both observed and simulated spectra for comparison. For other directions of $\mathbf{B}$ the spectrum is more complicated because the sites become inequivalent.

The intensity of the spectrum followed Curie's law, i.e., was proportional to $1/T$ as T increased, and decreased without change in linewidth until it became too small to measure at about 40 K. The total spectral intensity was independent of the orientation of the crystal in the magnetic field. Figure 4 shows the intensity dependence of the spectrum of NOC4, together with that of $P1$, as a function of microwave power for $\mathbf{B}$ parallel to $\langle 100\rangle$. The microwave power used strongly saturated the $P1$ spectrum, but the transitions of NOC4 were recorded near the turning point of the saturation curve.

B. Model for NOC4

Nitrogen is one of the few elements with an isotope of nearly 100% natural abundance with $I=1$, and is the only element likely to be at a significant stable impurity site in diamond. The center responsible for this spectrum clearly has two equivalent nitrogen atoms at sites of axial symmetry

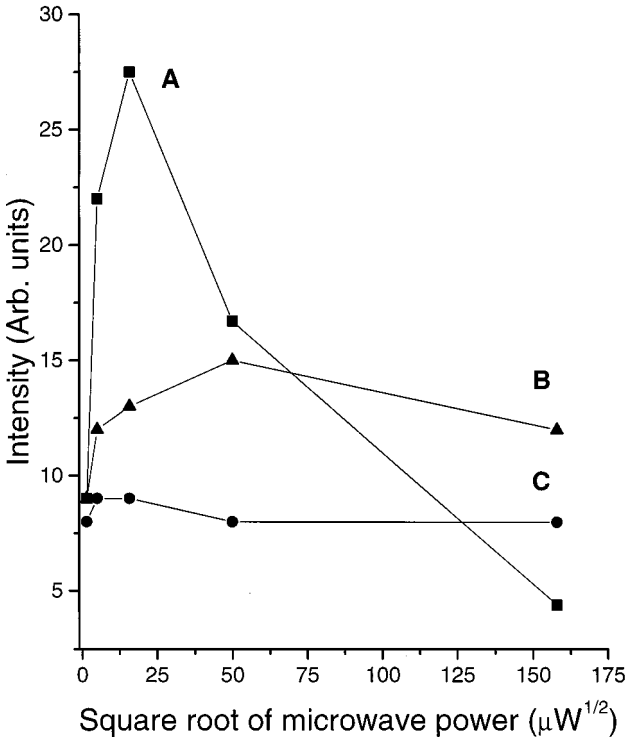

FIG. 4. EPR signal intensity as a function of microwave power for (*A*) the spectrum of $P1$ (squares), (*B*) the spectrum of NOC4 (triangles), and (*C*) the high-field spectrum (circles). The microwave frequency was approximately 9.6 GHz, and the measurements were made at room temperature using a TE_{104} rectangular cavity.

about $\langle 111\rangle$ directions, with the two axes randomly distributed among the possible $\langle 111\rangle$ directions.

It is unlikely that one could find a model for a system with a genuine g value which is isotropic and ~ 4 involving a defect with just two N atoms. However, it is possible to account for the observed spectrum in another way with a system described by the same spin Hamiltonian as Eq. (1), but with $S=1$ (and basis states $|M_S\rangle$), and with halved g and A values, as shown in the second line of Table II under NOC4. Suppose that the observed transition corresponds to $|+1\rangle \leftrightarrow |-1\rangle$. No $|\pm 1\rangle \leftrightarrow |0\rangle$ transitions are observed, but they could be obscured by the strong spectrum of $P1$. This indicates a system with two unpaired electrons. There are difficulties with this model, as generally one would expect a term $\mathbf{S}\cdot\mathbf{D}\cdot\mathbf{S}$ in the spin Hamiltonian. If the central field of the hyperfine lines were truly isotropic, this would imply that $D=0$. Then there would be zero transition probability for $|+1\rangle \leftrightarrow |-1\rangle$ transitions. However, if D were nonzero, both the line position and its intensity should be dependent upon the direction of **B**.[31]

The principal clue to the origin of the center is that the hyperfine structure parameters for the nitrogen atoms listed in Table I are identical to those of ^{14}N in the $P1$ center. This strongly suggests a model in which two $P1$ centers are loosely coupled by mutual interaction, expected to be dipole-dipole interaction $[\mathbf{S}_1\cdot\mathbf{J}(\mathbf{R})\cdot\mathbf{S}_2]$ at large distances and possibly with additional exchange interaction at shorter distances (with **R** the relative position of the two centers). If one could ignore the hyperfine interaction, the coupling of two identical systems with $S=1/2$ would lead to eigenstates $S=S_1+S_2=1$ or 0, with no transitions between $S=1$ and $S=0$.[31,32] Hence there would be a system with $S=1$, such as we observe. The hyperfine interaction mixes $S=0$ and 1 states.[33–35] The theory of such a model is discussed in the Appendix, where it has been assumed that the interaction between the two $P1$ centers does not modify the hyperfine parameters of the individual $P1$ centers, and that there is no significant interaction between the electron of one $P1$ center and the ^{14}N nucleus of the other.

The spin Hamiltonian for this system is

$$\mathcal{H}=g\mu_B\mathbf{B}\cdot(\mathbf{S_1}+\mathbf{S_2})+\mathbf{S_1}\cdot\mathbf{A_1}\cdot\mathbf{I_1}+\mathbf{S_2}\cdot\mathbf{A_2}\cdot\mathbf{I_2}+J_0\mathbf{S_1}\cdot\mathbf{S_2}+\mathbf{S_1}\cdot\mathbf{J}\cdot\mathbf{S_2}, \quad (3)$$

where the first term represents the electronic Zeeman interaction, and the next two terms the hyperfine interaction of each unpaired electron with its own nitrogen nucleus. It should be remembered that $\mathbf{A}_1$ and $\mathbf{A}_2$ may be oriented along the same or different $\langle 111\rangle$ directions. J_0 represents isotropic exchange, and the term in **J** represents the magnetic dipole-dipole interaction, but may also have a contribution from anisotropic exchange. For the moment, we will assume that we are concerned with fairly well-separated $P1$ centers, so that we can treat the term in **J** as purely dipolar, which means that the term in **J** depends upon a parameter $J=(\mu_0/4\pi)(\mu_B^2 g^2/R^3)$, where R is the separation of the two $P1$ centers, and functions of the angle θ between **B** and **R** [see Eq. (A3)]. We will discuss the justification of this assumption in the light of the results obtained. The detailed algebra for the derivation of energy levels and transitions is developed in the Appendix.

The electronic basis states for such a system are $|Ms_1, Ms_2\rangle$, and the half-field transition is between states $|++\rangle$ and $|--\rangle$, where for brevity we have written $|+\tfrac{1}{2},+\tfrac{1}{2}\rangle$ as $|++\rangle$ etc. In the Appendix we show that the $|++\rangle$ and $|--\rangle$ states do behave like the $|+1\rangle$ and $|-1\rangle$ states of an $S=1$ system, even when the hyperfine interaction is larger than the spin-spin interaction. The position and transition probability for this half-field transition are given in Eqs. (A14) and (A17). Both of these show a marked dependence on the angle θ between the applied magnetic field **B** and the direction **R**. No such angular dependence is observed. Nor is there a great multiplicity of lines observed, which one might expect from the range of possible values of **R**. The structure observed corresponds just to the hyperfine structure, with no structure due to different values of J.

Equations (A14) and (A17) show that sites with small values of R should have larger intensities and larger displacements. As R becomes larger, the displacements should become smaller and the lines should merge into a single line. When so merged, there would be no angular variation of intensity, since all values of θ contribute. It should be remembered that the hyperfine structure depends only upon ϕ, the relative orientation of **B**, and the four $\langle 111\rangle$ directions, so that for large values of R all orientations of **R** contribute to the same hyperfine line, and summation over θ averages out the angular variation. Equation (A10) shows that the hyperfine structure of such a pair is given by $\frac{1}{2}(A_1 m_1 + A_2 m_2)$, so,

for such a description, the spin Hamiltonian parameters are give by the third line in Table II under NOC4.

This we believe is the explanation for the properties of the NOC4 spectrum. It corresponds to the summation of intensities of $|++\rangle \leftrightarrow |--\rangle$ transitions for all possible pairs of $P1$ centers at greater separation than some limiting value of R where the lines lie outside the composite line for distant neighbors.

All of the components of this composite line are displaced to lower magnetic fields by the second order effects of J, so the aggregate line suffers a shift from the true half-field value. This accounts for the difference between the g value for $P1$ and that given for NOC4 in Table I. Experimentally this shift was found to be about 0.2 mT, which is consistent with the displacement lying within the composite linewidth of 0.3 mT. The observed linewidth puts an upper limit on the value of J for neighbors which are included in the composite line. The value of smallest $R=R_0$ is about 0.7 nm. No separate lines are observed for smaller values of R. This could be because the intensities of these individual pair lines are just too small. Note that this theory has been based on the assumption that R represents the distance between point dipoles. If the pair of $P1$ centers are oriented with their N-C bonds directed outwards, the separation of the constituent N_s could be considerably smaller than R.

As the angular function to be averaged is the same for all values of R (provided that we ignore the real structure of the diamond lattice), the line shape for each shell of neighbors is the same, but is scaled in displacement as (J^2/G) (where $G=g\mu_B B$) and in intensity as $(J/G)^2$. The maximum intensity $I(J)_{\max}=3.25(J/G)^2$ corresponds approximately to a maximum displacement $S(J)_{\max}=0.375(J^2/G)$. So for any value of J, $I(J)_{\max}=\alpha S(J)_{\max}$, where $\alpha=8.67$. For a concentration c of $P1$ sites, the probability that a neighbor has a value of R between R and $R+dR$ is $P(R)dR=4\pi cR^2dR$. The corresponding expression, regarding S as the variable and taking $J=AR^{-3}$, is

$$P(S)dS=-\left(\frac{2\pi\alpha_1 c}{3}\right)\left(\frac{0.372A^2}{G}\right)^{1/2}S^{-3/2}dS. \qquad (4)$$

So the total line intensity goes as

$$I(S)P(S)dS=-\left(\frac{4\pi\alpha_1 c}{3}\right)\left(\frac{0.372A^2}{G}\right)^{1/2}S^{-1/2}dS. \qquad (5)$$

This gives an intensity which decreases with shift, because the increase in $I(S)_{\max}$ is dominated by the fall in probability $P(S)$. $P(S)$ must be cut off when the shift ceases to be continuous or there are no more paramagnetic neighbors. The integrated intensity is

$$67\left(\frac{J(R_0)^2}{G}\right)^2(R_0/a_0)^3c, \qquad (6)$$

where R_0 is the smallest radius. The intensity of this line is thus about $0.7c$, which compares reasonably with the measured value. Note that individual pair lines at distance R_0 would have intensity $[J(R_0)^2/G]^2c=0.006c$, so resolved lines would be difficult to observe.

For these pair sites, one would expect transitions near $g=2$, corresponding to the transitions described by Eqs (A8) and (A9). However, pairs with $R>0.7$ nm would lie so close to the strong lines of the $P1$ spectrum that they would be unresolved in the wings of the lines of $P1$, and simply contribute to the linewidth.

IV. SPECTRA NEAR $g=2$: NOC1, NOC2, AND NOC3

A. Spectrum

The spectrum near $g=2$ (see Fig. 1) comprises the normal EPR from $P1$, and smaller signals for $W8$, $NE1$, and $NE4$. In addition to these four centers there are even weaker lines with about 10^{-3} of the peak-to-peak signal of P1. They occur in groups which have complicated angular dependences, but for **B** along $\langle 100\rangle$ they simplify into a pattern of lines of relative intensity 1:2:3:2:1 and equally spaced with a separation equal to half of the separation of the hyperfine lines of the $P1$ center. For other directions of **B** the patterns have lines which have separations which approximately correspond to half of the separation of the hyperfine lines of $P1$ in that direction (see Table I). Spectra from three distinctly different pair configurations have been identified and labeled NOC1, NOC2, and NOC3. The hyperfine structure is illustrated for salient directions in Fig. 5, and the complicated angular variation of the middle of the hyperfine structure for the many symmetry-related sites is shown in Fig. 6.

Although the portion of the angular variation which can be studied is too small for a complete fitting to a spin Hamiltonian, these spectra can be fitted to a spin Hamiltonian, with $S=1$, $I_1=I_2=1$,

$$\mathcal{H}=g\mu_B\mathbf{B}\cdot\mathbf{S}+D\{S_Z^2-\tfrac{1}{3}S(S+1)\}+\mathbf{S}\cdot(\mathbf{A_1}\cdot\mathbf{I_1}+\mathbf{A_2}\cdot\mathbf{I_2}), \qquad (7)$$

where the observed spectra correspond to transitions $|\pm 1\rangle \leftrightarrow |0\rangle$. The spin Hamiltonian parameters for the three sites are listed in Table II, as well as the angle Θ between the z axis for the term in D and $\langle 100\rangle$ and the principal directions of the axially symmetric **A** matrices.

B. Models for NOC1, NOC2, and NOC3

As for the NOC4 spectrum, the centers responsible for these spectra clearly have two equivalent nitrogen atoms, and, although it has been possible to measure only over a limited range of directions of **B**, they are consistent with nitrogen atom sites of axial symmetry about $\langle 111\rangle$ axes, but with each center corresponding to a different pair of $\langle 111\rangle$ axes. The observed hyperfine structure separations and spin Hamiltonian parameters are again nearly identical to those for ^{14}N in the $P1$ center. The intensities of the lines relative to those of $P1$ are about equal to c, the local concentration of $P1$.

This suggests that the centers also comprise pairs of interacting $P1$ centers (see Sec. II E). Again the measured hyperfine parameters suggest that the wave functions of the constituent $P1$ centers are not greatly perturbed by the interaction with one another. We can therefore describe them by

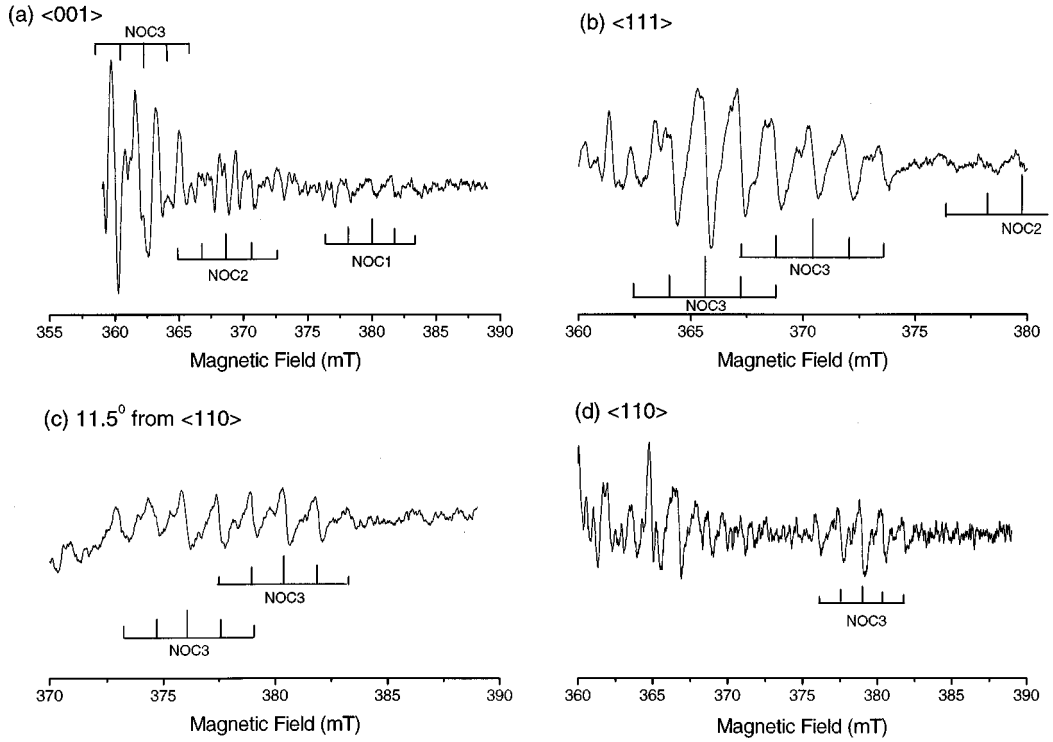

FIG. 5. EPR spectra of NOC1, NOC2, and NOC3 for **B** in the {011} plane, showing hyperfine structure: (a) for **B** along ⟨100⟩, (b) NOC2 and NOC3 for **B** along ⟨111⟩, (c) NOC3 for **B** at 11.5° from ⟨110⟩, and (d) NOC3 for **B** along ⟨110⟩. The microwave frequency was approximately 9.7 GHz, and the measurements were made at room temperature.

the spin Hamiltonian in Eq. (3). In the Appendix, we differentiate between two different types of transition in the pair spectra: (a) type *A*, corresponding to transitions $|++\rangle \leftrightarrow |+-\rangle$, $|-+\rangle$ and $|+-\rangle$, $|-+\rangle \leftrightarrow |--\rangle$, described by Eqs. (A6)–(A10); and (b) type *B*, corresponding to transitions $|++\rangle \leftrightarrow |--\rangle$, described by Eqs. (A11)–(A14). We suppose that for NOC1-3, we are observing type-*A* transitions described by Eq. (A10). The measured parameter *D* is related to the coupling parameter *J* [see Eq. (A3)]: $D = \frac{3}{2}J$.

On the assumption (to be discussed below) that the interaction is purely dipole-dipole, the separation *R* between the pairs can be calculated using Eq. (A3), and Θ gives the angle between **R** and ⟨100⟩. There are undoubtedly spectra from more distant pairs which cannot be recognized, as they have smaller values of $D(J)$ and so lie within the dense pattern of lines. The pairs which give rise to the NOC4 spectrum fall in this class.

The intensity of transitions in NOC1–NOC3 are independent of the value of θ, but unlike NOC4 the line positions are affected to first order in *J*, and so have large angular dependence. Therefore, the spectrum has a complicated angular dependence, and as the lines lie close to the spectrum of the much stronger lines from $P1$, it is difficult to follow their complete angular variation. The spectrum simplifies for **B** along high-symmetry directions, because the symmetry equivalence of related pair sites causes their lines to overlap. This both reduces the number of lines to be resolved, and also increases their intensity.

The criteria (a) and (b) described by Eqs. (A8) and (A9), and (A7), respectively, correspond roughly to spectra whose displacements are large or small relative to the hyperfine structure of $P1$. As those which are smaller are unlikely to be detectable among the ^{13}C hyperfine lines of $P1$, it is only type (b) we need to consider.

A crude identification of the observed pair species may be made from the value of $J(\frac{2}{3}D)$ and the angle Θ between the direction of maximum separation and ⟨100⟩, given in Table III, by assuming that it corresponds to dipole-dipole interaction between just the 67% electron density on the unique C atoms of the two $P1$ units, which we label C_a and C_b. This gives the separation *R* between these atoms in the fourth column of Table III. The fifth column gives the relative positions of undistorted lattice sites for C_a and C_b which is closest to the values of *R* and Θ: the sixth and seventh columns give the values of *R* and Θ for these sites. To refine this calculation requires taking into account the 25% electron density on the N atoms, and the elongation of the unique N-C bond in the $P1$ center.

The hyperfine interaction is related to the directions of the bonds C_a-N_a and C_b-N_b. The hyperfine interaction for each of the centers indicates that they do not correspond to a statistical distribution of all possible orientations of C_a-N_a and C_b-N_b, but to a special pair of directions for each observed pair center. The hyperfine structure shows whether C_a-N_a and C_b-N_b for an observed pair site with principal axes in the (110) plane lie in that plane or in the normal $\{1\bar{1}0\}$ plane. Neither NOC1 nor NOC2 has its $P1$ components oriented parallel to one another. Unfortunately, the hyperfine structure in the accessible region of the angular variation for NOC3 does not allow us to determine whether the $P1$ components are parallel or not, but only that they lie in a $(1\bar{1}0)$ plane. Hence we have considered both possibilities.

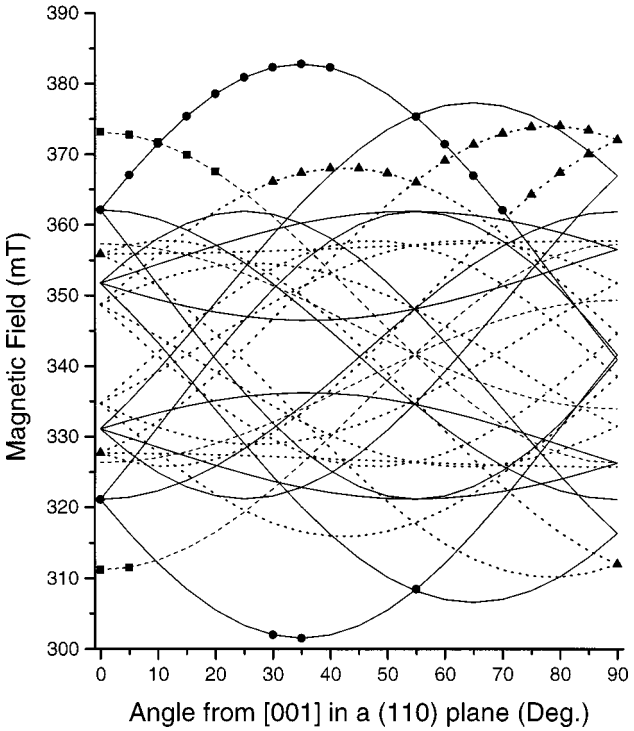

FIG. 6. Angular plot showing the position of the EPR transitions for NOC1, NOC2, and NOC3, when the magnetic field is rotated in a (110) plane away from [001]. The experimental data points (NOC1, squares; NOC2, circles; NOC3, triangles) are plotted at the central field of the nitrogen hyperfine structure on each allowed electronic transition. The broken curve shows the best fit to the NOC1 data, the solid curve shows the best fit to the NOC2 data, and the dotted curve shows the best fit to the NOC3 data. The simulated microwave frequency was 9.58 GHz.

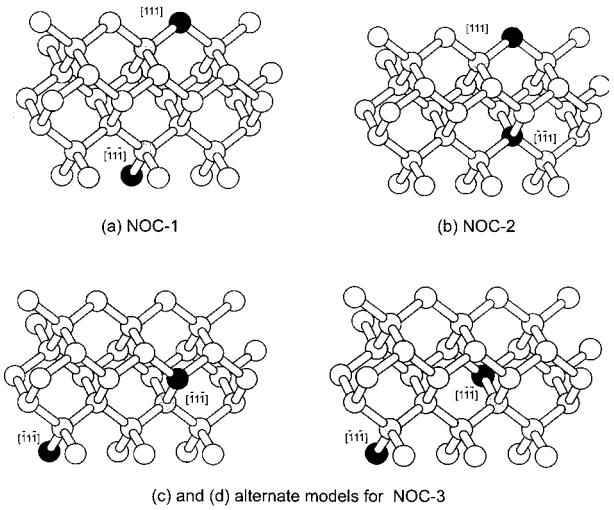

FIG. 7. Models of the $P1$ pair defects: (a) NOC1, (b) NOC2, and (c) and (d) the alternatives for NOC3. Heavily shaded atoms are nitrogen and lightly shaded atoms are carbon in the unique N-C_1 bond of $P1$.

Starting with the assumption that the fifth column in Table III correctly sites the atoms C_a and C_b, a next-order corrected value of J has been calculated for the possible positions of N_s atoms, consistent with the known directions of C_a-N_a and C_b-N_b, assuming that 25% of an unpaired electron is located on these N_s atoms at undistorted lattice sites; and the eigth column of Table III give the relative positions of N_a and N_b which gives the value of J closest to that observed, and this calculated value of J is given in the ninth column.

It should be remembered that this is a very crude calculation, which does not take account of lattice distortion, nor the distributed nature of the magnetic moments, and it ignores any nondipolar interactions; so one would not expect close correlation between calculated and experimental values of J. However, all of this evidence points to the identification of the measured nearby pair sites as shown in Table III. The only ambiguity is in the identification of NOC3. These sites are illustrated in Fig. 7.

One would expect such pair sites to give rise to weak type-B lines near the NOC4 spectrum, and from the known parameters one can calculate that they would be resolved from that spectrum for certain directions of **B**. Certainly no resolved lines are observed at positions predicted from the parameters determined from allowed pair spectra for closer neighbors. This is probably because the intensity of the lines is just too small.

The measured hyperfine structure splittings for these sites are not quite the same as half of those for the $P1$ center, indicating that the proximity of a second $P1$ center does slightly modify the distribution of spin density.

It should be emphasized that this interpretation *assumes* that the anisotropic part of the interaction between the $P1$ components is dipolar (any isotropic component would be undetected in the EPR measurements, unless J_0 were positive and large enough for the EPR active states to be thermally depopulated). However, observation of only three sites, and the measured orientation of the C_a-N_a and C_b-N_b

TABLE III. Parameters for the measured nearby pair spectra. See Sec. IV B for an explanation of the parameters.

Name	Experimentally determined parameters			Nearest C_a-C_b site			Best N_a-N_b site	Calculated J
	J (mT)	Θ (deg)	R (nm)	(C-C) (a_0/4)	Θ (deg)	R (nm)	(N-N) (a_0/4)	(mT)
NOC1	31.0	0	0.342	(0,0,4)	0	0.354	(2,0,6)	38.5
NOC2	40.7	35	0.312	(2,2,4)	35.3	0.433	(0,0,4)	42.1
NOC3	31.4	78.5	0.341	(3,3,1)	76.7	0.385	(3,3,3)	34.9
							(5,1,3)	34.4

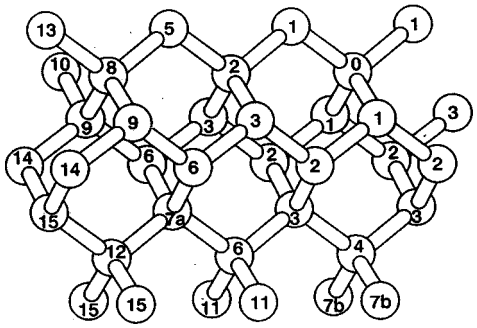

FIG. 8. A view of the diamond lattice from slightly off the $[1\bar{1}0]$ direction with the (110) direction almost in the plane of the paper, which shows the relative positions of atom 0 and its nth-nearest neighbors, labeled n.

bonds, is independent of this assumption. The linkages between the nearest N or C atom of the two $P1$ constituents is at least three bonds long, which makes it unlikely that anisotropic exchange is significant.

C. Discussion of neighbor sites

Even though the tetrahedrally bonded crystal structure of diamond is basically very simple (it is face-centered-cubic with a two-atom basis), it is difficult to visualize the relative positions of the atoms. Since the principal spectra we wish to discuss involve pairs of nitrogen atoms in substitutional sites at different distances, Fig. 8 and Table IV enable the reader to visualize the pair structure. In Fig. 8 the atoms are labeled with a number indicating their ranking as neighbors of the atom labeled 0 in order of increasing distance R from the atom labeled 0. Table IV gives, for each rank of neighbor, the relative coordinates in the cubic crystal axes in units of $a_0/4$, the value of R, and the number of symmetry-related copies of each pair site in the undistorted lattice.

As each paramagnetic constituent of the pairs observed comprises two atomic sites, N_s and one neighboring C atom, the principal constituents of the centers we observe involve four atoms: i.e., two distinct N-C fragments. This leads to a larger number of symmetry-related pair sites than would be obtained if only the relative positions of the N_s atoms were relevant.

TABLE IV. Neighbor sites, ranked in order of distance R, showing relative coordinates in the cubic crystal axis system in units of $a_0/4$, the value of R, and the number of symmetry related sites. See Fig. 8 and text for further details.

n	Coordinates	R (nm)	Number of sites
1	(1,1,1)	0.154	4
2	(2,2,0)	0.252	12
3	(3,1,1)	0.296	12
4	(4,0,0)	0.357	6
5	(3,3,1)	0.389	12
6	(4,2,2)	0.437	24
7a	(3,3,3)	0.464	4
7b	(5,1,1)	0.464	12
8	(4,4,0)	0.505	12
9	(5,3,1)	0.528	24
10	(6,2,0)	0.565	24
11	(5,3,3)	0.585	12
12	(4,4,4)	0.618	8

The concentration of NOC4 appears to correspond to a statistical occupation of pairs of carbon atom sites by N_s, and we argue below that it is possible to explain the concentration of NOC1 and NOC3 on the same assumption. Does this indicate that all possible sites for N_s pairs in the crystal are equally probable? At the temperature of incorporation, the extra antibonding electron is free to tunnel between all N-C orbitals, and so will take up whatever orbital is favored by electrostatic or strain energy. The data for NOC4 suggest that at large distances all orientations of N-C occur, but the data for $P1$ pairs at smaller distances suggest that unique orientations are favored.

The concentration of A centers is much higher than the statistical occupation of nearest neighbor sites, so considerable aggregation has occurred. Calculations[29] for second- and third-neighbor pairs show that electrons occupy orbitals which have some overlap and are spin paired to give an $S=0$ ground state. Hence we have no measure of the density of N_s at second- and third-neighbor positions, so we do not know whether they have suffered collapse into A centers, which reduces their population. The concentration we measure for NOC2, corresponding to fourth-neighbor N_s at (0,0,4), is much smaller than one would expect for a random distribution, which may suggest erosion of their concentration due to partial coalescence to form A centers. The situation for fifth neighbors (planar N-C-C-N) is different, since the C-C bond lies between the two N atoms, but overlap is again maximized by the electrons occupying the two parallel N-C bonds, for which calculations[29] predict that $S=0$, so we have no information about these sites since we cannot detect them.

It is unfortunate that the accessible data does not enable us to say whether the site NOC3 is due to seventh or ninth neighbors. However, as there are only four seventh-neighbor sites and 24 ninth-neighbor sites, the large intensity of the lines makes it much more likely that it is ninth neighbors, when the intensity would be consistent with a statistical distribution of N_s: the low relative concentration of seventh neighbors and the almost identical value of D makes it possible that both sites exist, but that the latter is too weak for us to resolve.

The concentration of tenth-neighbor sites, which gives rise to NOC2, is very much less than would be expected statistically, if they formed a special site. However, if at this distance all orientations of C_a-N_a and C_b-N_b are possible, the intensity of the observed NOC2 site is credible. All other sites formed by this position of N_s pairs, including two which correspond to nearest C_a-C_b atoms at (2,2,4), have too small a value of D to be observed.

We should try to explain why we do not observe other sites. It is difficult to understand why sites at sixth neighbor and beyond should correspond to $S=0$ if fourth-neighbor sites do not. That we do not observe the spectra from such sites must indicate that C_a and C_b must be further apart than they are in the sites we do observe. To be clearly recognized and distinguished, among the complicated angular dependence of those pair lines we do observe, any other would

have to correspond to a separation between C_a and C_b of less than $R=0.34$ nm, which puts a lower limit on the observable separation between N_s components of about 0.6 nm (11th neighbors). It is possible that for the pair sites for N_s we do not see in this range C_a and C_b have greater separation than the N_a and N_b atoms, but it is difficult to formulate any principle for deciding why. What is the reason for there being specific $P1$ sites for these near neighbors, rather than a random distribution? At close distance this could be due to both strain around the elongated N-C bond and electrostatic interaction between the $P1$ electric dipoles. For particular relative positions of the two N_s atoms, this would influence the direction taken up by the unique N-C bonds. However, we have not been able to find any principle of calculation which consistently predicts the pair sites we find, and those we do not find, at close distance. As the N_s atoms become more separated, the effects of strain and electrostatic interactions become less important, and so all orientations will occur.

V. HIGH-FIELD SPECTRUM

The high-field spectrum (see Fig. 3) can be described by the spin Hamiltonian [Eq. (1)] with $S=1/2$, $I=1$, and parameters listed in Table I. The three line hyperfine structure is again indicative of ^{14}N. However this would require a g value of 1 which is unlikely for a center involving one nitrogen atom. The high-field spectrum is an exact replica of the spectrum of $P1$ having identical hyperfine structure, but displaced to be centered at nearly double the magnetic field. This suggests that the $P1$ center is responsible for this spectrum.

One explanation for this spectrum is that it is a two photon transition excited between the energy levels, which results in flipping the spin of $P1$. However, this spectrum has not been thoroughly examined, and its properties will be discussed in a later publication.

VI. CONCLUSIONS

EPR measurements in diamonds with high concentration of N_s have shown two types of spectra due to interacting pairs of N_s: one spectrum close to that of the $P1$ center near $g=2$, and the other at about half the $P1$ resonant magnetic field. The former shows three different pair sites (NOC1, NOC2, and NOC3), and the closest distance at which the pairs behave like spin $S=1$ is for the N_s atoms separated by a_0 (0.357 nm) in NOC2. The low-field center (NOC4) corresponds to a superposition of pairs with all possible orientations of the constituent $P1$ centers, at many different sites of separation greater than about 0.7 nm.

The synthetic diamonds studied have an unusually high concentration of A centers, which may have been produced by aggregation of nitrogen atoms diffusing on the surface of the growing crystal.

EPR spectra have also been observed at high field, which probably corresponds to two photon transitions in isolated N_s.

ACKNOWLEDGMENTS

This work was supported by the Engineering and Physical Sciences Research Council (EPSRC) Grants Nos. GR/H33053 and GR/K1562.6, and by the Russian Foundation of Basic Research Grant No. 98-05-65283. D.J.T. thanks Merton College, Oxford, and Linacre College, Oxford, for financial support. M.E.N. thanks EPSRC for support and V.A.N and A.P.Y. thank the Royal Society for support.

APPENDIX: THEORY OF THE PAIR SPECTRA

The spin Hamiltonian we have proposed to describe a pair of loosely interacting $P1$ centers is given in Eq. (3). The last two terms may be expanded:

$$J_0\mathbf{S_1}\cdot\mathbf{S_2}=J_0S_{1Z}S_{2Z}+\tfrac{1}{2}J_0(S_{1+}S_{2-}+S_{1-}S_{2+}), \quad \text{(A1)}$$

$$\begin{aligned}\mathbf{S_1}\cdot\mathbf{J}\cdot\mathbf{S_2}=&J_{ZZ}S_{1Z}S_{2Z}+J_{+-}(S_{1+}S_{2-}+S_{1-}S_{2+})\\&+J_{++}(S_{1+}S_{2+}+S_{1-}S_{2-})\\&+J_{Z+}(S_{1+}S_{2Z}+S_{1Z}S_{2+}+S_{1-}S_{2Z}+S_{1Z}S_{2-}).\end{aligned} \quad \text{(A2)}$$

If $\mathbf{J}$ is purely dipolar, we can express $\mathbf{J}$ in terms of the separation R between the dipoles and the angle θ between $\mathbf{R}$ and $\mathbf{B}$ as follows:

$$J_{ZZ}=(1-3\cos^2\theta)J, \quad J_{+-}=\frac{1}{4}(3\cos^2\theta-1)J=-\frac{1}{4}J_{ZZ},$$

$$J_{++}=-\frac{3}{4}\sin^2\theta J, \quad J_{Z+}=-\frac{3}{2}\cos\theta\sin\theta J,$$

where

$$J=\frac{\mu_0}{4\pi}\frac{\mu_B^2g^2}{R^3}. \quad \text{(A3)}$$

The axis of quantization of $\mathbf{S}$ has been chosen to be along $\mathbf{B}$, so that the first term in Eq. (3) becomes $g\mu_B(S_{1Z}+S_{2Z})B$.

Formally, we should diagonalize the 36×36 matrix spanning (S_1,S_2,I_1,I_2). However, because $A\ll g\mu_BB$ we can simplify the calculation. By an appropriate choice of quantization axis for $\mathbf{I_i}$, the terms in $S_{iZ}I_{i+}$ and $S_{iZ}I_{i-}$ can be made zero. Then one has a diagonal term $A_iS_{iZ}I_{iZ}$, where $A_i=(A_\parallel^2\cos^2\phi_i+A_\perp^2\sin^2\phi_i)^{1/2}$, and ϕ_i is the angle between $\mathbf{B}$ and the principal direction of $\mathbf{A_i}$. All of the other hyperfine terms couple states which are separated by $g\mu_BB$, and so produce only small admixtures of states of order $A/g\mu_BB$ and energy shifts of order $A^2/g\mu_BB$, which can be ignored. Note that this may involve choosing different axes of quantization for $\mathbf{I_1}$ and $\mathbf{I_2}$. This solution means that the hyperfine terms reduce to diagonal matrix elements $A_1M_1m_1+A_2M_2m_2$, and the matrix can be factorized into 4×4 matrices for each value of (m_1,m_2):

$$
\begin{array}{cccc}
 & |++\rangle & |+-\rangle & |-+\rangle & |--\rangle \\
|++\rangle & G+\frac{1}{2}A_{++}+Z & \frac{1}{2}J_{Z+} & \frac{1}{2}J_{Z+} & J_{++} \\
|+-\rangle & -\frac{1}{2}J_{Z+} & \frac{1}{2}A_{+-}-Z & \frac{1}{2}J_0-\frac{1}{4}J_{ZZ} & \frac{1}{2}J_{Z+} \\
|-+\rangle & -\frac{1}{2}J_{Z+} & \frac{1}{2}J_0-\frac{1}{4}J_{ZZ} & -\frac{1}{2}A_{+-}-Z & \frac{1}{2}J_{Z+} \\
|--\rangle & J_{++} & -\frac{1}{2}J_{Z+} & -\frac{1}{2}J_{Z+} & -G-\frac{1}{2}A_{++}+Z,
\end{array}
$$

where $G=g\mu_B B$, $A_{++}=(A_1m_1+A_2m_2)$, $A_{+-}=(A_1m_1-A_2m_2)$, and $Z=\frac{1}{4}(J_0+J_{ZZ})$.

For $P1$ pairs, $J \ll g\mu_B B$, so the central 2×2 matrix can be solved exactly, and perturbation theory can be used for the remaining part of the problem. The eigenstates and energies of the central two states are:

$$\cos\alpha|+-\rangle+\sin\alpha|-+\rangle, \quad E_1=-\tfrac{1}{4}(J_0+J_{ZZ})+X, \tag{A4}$$

$$\sin\alpha|+-\rangle-\cos\alpha|-+\rangle, \quad E_2=-\tfrac{1}{4}(J_0+J_{ZZ})-X, \tag{A5}$$

where $\tan(2\alpha)=(J_0-\frac{1}{2}J_{ZZ})/(A_1m_1-A_2m_2)$ and $X=\frac{1}{2}[(A_1m_1-A_2m_2)^2+(J_0-\frac{1}{2}J_{ZZ})^2]^{1/2}$. To first order, the transitions $|++\rangle\leftrightarrow|+-\rangle$, $|-+\rangle$, which we label type A, occur when

$$h\nu=G+\tfrac{1}{2}(J_0+J_{ZZ})+\tfrac{1}{2}(A_1m_1+A_2m_2)\mp X, \tag{A6}$$

$$h\nu=G-\tfrac{1}{2}(J_0+J_{ZZ})+\tfrac{1}{2}(A_1m_1+A_2m_2)\pm X, \tag{A7}$$

with intensities for a microwave magnetic field $\mathbf{B}_1$ applied perpendicular to $\mathbf{B}$ given by matrix elements of $\frac{1}{2}g\mu_B B_1(S_{1+}+S_{1-}+S_{2+}+S_{2-})$. This term is proportional to $\cos^2 2\alpha$ for the upper sign and to $\sin^2 2\alpha$ for the lower sign. It is interesting to consider two extreme cases.

(a) When $(A_1m_1-A_2m_2)\gg(J_0-\frac{1}{2}J_{ZZ})$, $\cos 2\alpha=0$,

$$h\nu=G\pm\tfrac{1}{2}(J_0+J_{ZZ})+A_1m_1 \tag{A8}$$

or

$$h\nu=G\pm\tfrac{1}{2}(J_0+J_{ZZ})+A_2m_2. \tag{A9}$$

(b) When $(A_1m_1-A_2m_2)\ll(J_0-\frac{1}{2}J_{ZZ})$, $\cos 2\alpha=1$,

$$h\nu=G\pm\tfrac{3}{4}J_{ZZ}+\tfrac{1}{2}(A_1m_1+A_2m_2). \tag{A10}$$

These equations will be changed by the relatively small second order effects of off-diagonal elements of $\mathbf{J}$, and, since there is a considerable angular variation of the spectrum through J_{ZZ}, these changes can be ignored.

The hyperfine coupling term appearing in Eq. (A6) is exactly the same as for an isolated $P1$ center. When the spin-spin coupling is strong, a factor of $\frac{1}{2}$ appears in front of the $(A_1m_1+A_2m_2)$ term [see Eq. (A7)]. This factor appears because the electron spins are strongly coupled and the nuclear spin vector moment must be projected onto the resultant electron spin vector.

To this order, transitions $|++\rangle\leftrightarrow|--\rangle$, which we label type B, have zero intensity. If $G\gg J_0$ or $\mathbf{J}$, the effects of $\mathbf{J}$ on the relevant states ($|++\rangle$ and $|--\rangle$), calculated using perturbation theory, do not depend upon the value of α. The energies of the states are

$$E_{++}=G+\frac{1}{2}(A_1m_1+A_2m_2)+\frac{1}{4}(J_0+J_{ZZ})+\frac{(J_{Z+})^2}{2G}+\frac{(J_{++})^2}{2G}, \tag{A11}$$

$$E_{--}=-G-\frac{1}{2}(A_1m_1+A_2m_2)+\frac{1}{4}(J_0+J_{ZZ})-\frac{(J_{Z+})^2}{2G}-\frac{(J_{++})^2}{2G}. \tag{A12}$$

Thus the transition occurs when

$$h\nu=2G+(A_1m_1+A_2m_2)+\frac{(J_{Z+})^2}{G}+\frac{(J_{++})^2}{G}. \tag{A13}$$

The position of the line is given by

$$G=\frac{1}{2}h\nu-\frac{1}{2}(A_1m_1+A_2m_2)-\frac{9}{8}\frac{J^2}{G}\cos^2\theta\sin^2\theta-\frac{9}{32}\frac{J^2}{G}\sin^4\theta. \tag{A14}$$

at approximately half the field for the transitions described by Eqs. (A5)–(A7).

The states are, to first order of perturbation theory,

$$|++\rangle^* \Rightarrow |++\rangle + \frac{J_{Z+}}{2G}|+-\rangle + \frac{J_{Z+}}{2G}|-+\rangle + \frac{J_{++}}{2G}|--\rangle, \tag{A15}$$

$$|--\rangle^* \Rightarrow |--\rangle + \frac{J_{Z+}}{2G}|+-\rangle + \frac{J_{Z+}}{2G}|-+\rangle - \frac{J_{--}}{2G}|--\rangle, \tag{A16}$$

with the transition probability

$$\left[{}^*\langle ++| \frac{1}{2} g\mu_B B_1 (S_{1+} + S_{1-} + S_{2+} + S_{2-}) |--\rangle^* \right]^2 = \left[\frac{1}{2} g\mu_B B_1 \frac{3\cos\theta \sin\theta J}{G} \right]^2. \tag{A17}$$

Type-A transitions have probabilities proportional to $[\frac{1}{2} g\mu_B B_1]^2$, so relative to the type-A transitions, the probability of type-B transitions is

$$\left[\frac{3\cos\theta \sin\theta J}{G} \right]^2. \tag{A18}$$

Thus both the intensity and position of the type-B lines depend upon the angle θ, between **B** and **R**. The intensity has a maximum of $3.25(J/G)^2$ at $\theta = \pi/4$ near where the displacement reaches a maximum value of $0.375J^2/\mathrm{G}$. In contrast, the hyperfine structure does not depend upon θ, but only upon the angles ϕ_1 and ϕ_2.

*Author to whom correspondence should be addressed.

[1] W.V. Smith, P.P. Sorokin, J.I. Gelles, and G.I. Lasher, Phys. Rev. **115**, 1546 (1959).

[2] C.A.J. Ammerlaan, in *Semiconductors. Impurities and Defects in Group IV Elements and III-V compounds*, edited by O. Madelung and M. SchulZ, Landolt-Börnstein, New Series, Group III, Vol. 22, Pt. (b) (Springer, Berlin 1990), pp. 117–206.

[3] M. Ya Shcherbakova, V.A. Nadolinny, and E.V. Sobolev, J. Struct. Chem. **19**, 261 (1978).

[4] J.A. van Wyk and G. Woods, J. Phys.: Condens. Matter **5**, 5901 (1995).

[5] G. Davies, Chem. Phys. Carbon **3**, 1 (1997).

[6] *Properties and Growth of Diamond*, edited by G. Davies (INSPEC, London, 1994).

[7] R.M. Chrenko, R.E. Tuft, and H.M. Strong, Nature (London) **270**, 141 (1977).

[8] T. Evans and Z. Qi, J. Phys. C **14**, L379 (1981).

[9] T. Evans, in *The Properties of Natural and Synthetic Diamond*, edited by J.E. Field (Academic, London 1992), Chap. 6.

[10] A.T. Collins, J. Phys.: Condens. Matter **11**, L471 (1978); *ibid.* **13**, 2641 (1980).

[11] I. Kiflawi, H. Kanda, D. Fisher, and S.C. Lawson, Diamond Relat. Mater. **6**, 1643 (1997).

[12] D. Fisher and S.C. Lawson, Diamond Relat. Mater. **7**, 299 (1998).

[13] V.A. Nadolinny and A. P. Yelisseyev, Diamond Relat. Mater. **3**, 17 (1993).

[14] V.A. Nadolinny and A.P. Yelisseyev, Diamond Relat. Mater. **3**, 1196 (1994).

[15] A.P. Yelisseyev and V.A. Nadolinny, Diamond Relat. Mater. **4**, 177 (1995).

[16] V.A. Nadolinny, A.P. Yelisseyev, O.P. Yuryeva, and B.N. Feigelson, Appl. Magn. Reson. **12**, 543 (1997).

[17] Yu.N. Polyanov, I.Yu. Malinovsky, Yu.M. Borzdov, A.F. Khokhryanov, A.I. Chepurov, A.A. Godovikov, and N.V. Sobolev, Dokl. Akad. Nauk SSSR **315**, 1221 (1990) [Sov. Phys. Dokl. **35**, 324 (1991)].

[18] A. Yelisseyev, V. Nadolinny, B. Feigelson, S. Terentyev, and S. Nosukhin, Diamond Relat. Mater. **5**, 1113 (1996).

[19] J.H.N. Loubser and W.P. van Rynfeld, Nature (London) **211**, 517 (1966).

[20] M.I. Samoilovich, G.N. Bezrukov, and U. Butuzov, Pis'ma Zh. Éksp. Teor. Fiz. **14**, 551 (1971) [JETP Lett. **14**, 379 (1971)].

[21] J. Isoya, H. Kanda, J.R. Norris, and M.K. Bowman, Phys. Rev. B **41**, 3905 (1990).

[22] J.A. van Wyk, E.C. Reynhard, G.L. High, and I. Kiflawi, J. Phys. D **30**, 1790 (1997).

[23] D.F. Talbot-Ponsonby (private communication).

[24] A. Cox, M.E. Newton, and J.M. Baker, J. Phys. Condens. Matter **4**, 8119 (1992).

[25] S.G. Zhang, M.E. Zvanut, Y.K. Vohra, and S.S. Vagarali, Appl. Phys. Lett. **23**, 2951 (1994).

[26] P. R. Briddon, M. I. Heggie, and R. Jones, in *Proceedings of the Second International Conference on New Diamond Science and Technology 1991*, edited by R. Messier, T. J. Glass, J. E. Butler and R. Roy, MRS Symposia Proceedings No. 18 (Materials Research Society, Pittsburgh, 1991), p. 63.

[27] S. A. Kajihara, A. Antonelli, J. Bernholc, and R. Car, Phys. Rev. Lett. **66**, 2010 (1991).

[28] R. Jones, P. R. Briddon, and S. Oberg, Philos. Mag. Lett. **66**, 67 (1992).

[29] P. Bridden (private communication).

[30] J.H. Van Vleck, Phys. Rev. **74**, 1168 (1948).

[31] A. Abragam and B. Bleaney, *Electron Paramagnetic Resonance in Transition Ions* (Clarendon Press, Oxford, 1970).

[32] J. Owen, J. Appl. Phys. **32**, 213S (1961).

[33] J.M. Baker, Rep. Prog. Phys. **34**, 109 (1971).

[34] J.M. Baker, Phys. Rev. **136**, A1341 (1964).

[35] D.M.S. Bagguley and J. Owen, Rep. Prog. Phys. **20**, 304 (1957).